Gümüşhane University Journal of Science

GUFBD / *GUJS* (2025) 15(4): 1209-1221 doi: 10.17714/gumusfenbil.1779865 Research Article

Correlation between structural modifications and levitation performance in PAni-addition MgB_2 bulk superconductors

PAni katkılı MgB_2 külçe süperiletkenlerde yapısal modifikasyonlar ve levitasyon performansı arasındaki korelasyon

Tuğba BAYAZIT*

Central Research Laboratory, Recep Tayyip Erdogan University, 53100 Rize, Turkey

• Received: 08.09.2025 • Accepted: 01.12.2025

Abstract

In this study, bulk MgB_2 superconductors with varying polyaniline (PAni) contents (0–6 wt%) were synthesized via a closed-tube method and heat-treated at 850 °C under Ar atmosphere. Structural characterization by X-ray diffraction revealed that increasing PAni content led to systematic decreases in lattice parameters (a, c), interplanar spacing d (101), and unit cell volume, attributed to partial carbon substitution from PAni decomposition. This substitution, due to the smaller atomic radius of carbon compared to boron, modifies the crystal lattice and influences electronic structure. Crystallite size, dislocation density, and lattice strain calculations indicated that low-to-moderate PAni additions increase defect density and microstrain, potentially enhancing flux pinning. SEM analysis showed notable microstructural changes, including reduced porosity and improved homogeneity at lower adding, while higher contents promoted grain growth. Magnetic levitation force measurements under field-cooled (FC) and zero-field-cooled (ZFC) conditions showed that optimal PAni additions (4.5–6 wt%) improved the maximum levitation force in FC mode, while higher adding levels caused a decline in the initial force in ZFC mode, as observed at both 20 K and 25 K. The results establish a direct link between lattice parameter modification and levitation performance, offering insights for tailoring MgB_2-based superconductors for magnetic levitation applications.

Keywords: Lattice parameter, Magnetic levitation force, MgB_2 bulk superconductor, Polyaniline addition

Öz

Bu çalışmada, değişken polianilin (PAni) içeriklerine (0-6 ağırlık%) külçe MgB_2 süperiletkenleri kapalı tüp yöntemi ile sentezlendi ve Ar atmosferinde 850 °C'de ısıl işleme tabi tutuldu. X-ışını kırınımı ile yapısal karakterizasyon, artan PAni içeriğinin kafes parametrelerinde (a, c), düzlemler arası aralık d'de (101) ve birim hücre hacminde sistematik azalmalara yol açtığını, bunun da PAni ayrışmasından kaynaklanan kısmi karbon ikamesine atfedildiğini ortaya koydu. Bor ile karşılaştırıldığında karbonun daha küçük atom yarıçapından kaynaklanan bu ikame, kristal kafesini değiştirir ve elektronik yapıyı etkiler. Kristalit boyutu, dislokasyon yoğunluğu ve örgü zorlanması hesaplamaları, düşük ila orta düzeyde PAni ilavelerinin kusur yoğunluğunu ve mikrogerinimi artırarak potansiyel olarak akı sabitlemesini iyileştirdiğini gösterdi. SEM analizi, daha düşük katkılamada azaltılmış gözeneklilik ve iyileştirilmiş homojenlik de dahil olmak üzere önemli mikro yapısal değişiklikler gösterdi, daha yüksek içerikler ise tane büyümesini destekledi. Alan soğutmalı (FC) ve sıfır alan soğutmalı (ZFC) koşullar altında manyetik levitasyon kuvveti ölçümleri, optimum PAni ilavelerinin (%4,5-6 ağırlık) FC modunda maksimum levitasyon kuvvetini iyileştirdiğini, daha yüksek katkılama seviyelerinin ise hem 20K hem de 25K'de gözlemlendiği gibi ZFC modunda başlangıç kuvvetinde bir düşüşe neden olduğunu göstermiştir. Sonuçlar, kafes parametresi modifikasyonu ile levitasyon performansı arasında doğrudan bir bağlantı kurarak, MgB_2 bazlı süperiletkenlerin manyetik levitasyon uygulamalarına uyarlanması için fikirler sunmaktadır.

Anahtar kelimeler: *Örgü parametreleri, Manyetik kaldırma kuvveti, MgB_2 külçe süperiletkeni, Polyaniline katkısı*

1. Introduction

Since its discovery in 2001 (Nagamatsu et al., 2001), magnesium diboride (MgB_2) has attracted significant attention due to its relatively high superconducting transition temperature (Tc≈39 K) (Zhang et al., 2015),

*Tuğba BAYAZIT; tugba.bayazit@erdogan.edu.tr

hexagonal crystal structure with space group P6/mmm (Jorgensen et al., 2001), cost-effectiveness of materials (Shumaila et al., 2017) and well-connected grain boundaries (Shadab & Miryala, 2024), the distinct multiple superconducting energy gaps (Xi, 2008), compared to copper-oxide (cuprate) high-temperature (HT_c) superconductors ($YBa_2Cu_3O_{7-\delta}$ (YBCO), $Bi_2Sr_2CaCu_2O_8$ (BSCCO), etc.)

MgB_2, owing to its characteristic superconducting properties, is considered an important candidate for high-tech applications such as magnetic levitation systems, magnetic resonance devices, current-limiting units, and superconducting power equipment (Braccini et al., 2007; Güner, 2020; Savaşkan et al., 2019). In particular, large-scale applications such as MRI magnets, fault current limiters, and solenoids have demonstrated the technological feasibility of MgB_2 conductors (Braccini et al., 2007).

One of the most important challenges encountered in the practical applications of bulk MgB_2 is increasing the critical current density (J_c), flux pinning properties, and mechanical strength without significantly decreasing the transition temperature (T_c). To this end, various addition methods have been investigated, including carbon-based compounds, metal elemental dopants (such as Ag, Mg, Au), and organic dopants. For example, the addition of silver has been reported to enhance levitation performance by strengthening grain connectivity and improving the microstructure (Güner, 2020), Carbon-containing dopants (such as malic acid or pyrene) can improve both T_c and flux pinning ability by creating additional flux-pinning centers (Erdem et al., 2020). Some studies have also shown that adding excess magnesium reduces MgO impurity formation and improves superconducting grain connectivity (Zhang et al., 2015).

In the last few years, conducting polymers, with polyaniline (PAni) being one of the most studied, have attracted attention as novel additives for superconducting materials. Polyaniline (PAni, C_6H_7N) is a conducting polymer and an organic semiconductor characterized by a conjugated π–electron backbone that enables charge delocalization. Its electrical conductivity originates primarily from protonic acid doping, which converts the insulating emeraldine base form into the conductive emeraldine salt state (Stejskal et al., 2002). PAni is particularly attractive due to its easy and cost-effective synthesis (Prasanna et al., 2016), stability in air, and relatively high electrical conductivity (Soysal & Çıplak, 2023). When blended into a superconducting matrix, it can act as a conductive bond between grains, improving the homogeneity of the material and, in some cases, leading to better electrical and mechanical performance. Research on PAni/MgB_2 composites has shown changes in the microstructure, higher conductivity, and, in some reports, increased flux stabilization (Shumaila et al., 2014). The tendency of PAni to form uniform coatings or occupy grain boundary regions is thought to aid current transfer and maintain greater structure stability (Shumaila et al., 2017).

Even though earlier findings on PAni have been encouraging, its effect on bulk MgB_2 superconductors, particularly in relation to structure, morphology, and levitation force, has not been studied in much detail. Most of the existing literature deals with thin films, nanowires, or MgB_2 combined with PAni for electronic purposes, for instance in field emission devices, rather than for bulk superconducting levitation (Shumaila et al., 2019). For this reason, it is important to investigate how PAni influences phase development, grain linking, surface features, and magnetic levitation behaviour in bulk MgB_2, as this would give a clearer picture of its suitability for larger-scale superconducting uses.

In this study, bulk MgB_2 samples with varying PAni ine lattice parameters and assess structural changes induced by the polymer incorporation. Scanning electron microscopy (SEM) was employed to examine the microstructural features, while levitation force measurements were performed to evaluate magnetic performance. The primary aim is to elucidate the relationship between the PAni-induced modifications in the crystal lattice and the resulting variations in levitation force, thereby providing deeper insight into the role of PAni as a functional additive for optimizing MgB_2-based levitation systems.

2. Material and method

A series of MgB_2 samples with PAni concentrations of 0, 1.5, 3, 4.5, and 6 wt% were synthesized via solid-state processing. Amorphous boron (B) (>95%, Aldrich), magnesium (Mg) powder (99.8%, −325 mesh, Alfa Aesar), and polyaniline (PAni, High surface area conducting polyaniline, Sigma, Aldrich) were weighed in stoichiometric ratios, mixed thoroughly, and pressed into disk-shaped pellets (13 mm diameter, ~1.5 g). The pellets were then sintered at 850 °C in a sealed tube furnace under an argon atmosphere.

Before sintering, the powder mixture in the appropriate stoichiometric ratio was mixed in an agate mortar for approximately 30 minutes (Fig. 1a). The powder mixture was pressed under 2 bar pressure (Fig. 1b) and turned into a disk (Fig. 1c).

Figure 1. Preparation process of MgB_2–PAni bulk samples: (a) mixing precursor powders in an agate mortar, (b) pressing under 2 bar to form pellets, and (c) final pellet shape before heat treatment

The bulk MgB_2 samples with various PAni contents were synthesized by heating the precursor mixtures from room temperature to 850 °C at a rate of 5 °C/min, holding them at 850 °C for 1.5 h, and then cooling to room temperature at the same rate under a 1.5 bar argon atmosphere.

The crystal structures of the samples were analyzed using a Rigaku-SmartLab X-ray diffractometer (XRD) equipped with a Cu-Kα source (λ = 1.5408 Å), operated at 40 kV and 30 mA under ambient conditions. To ensure that the diffraction originated solely from the thin film layer, measurements were performed in parallel beam geometry with a fixed omega angle of 3° applied to the X-ray tube. This configuration effectively suppressed unwanted signals from the amorphous substrate.

Surface morphology and elemental composition were characterized using a scanning electron microscope (JEOL JSM 6610), coupled with an energy-dispersive X-ray spectroscopy (EDS) system (Oxford Instruments Inca X-act). To eliminate surface charging and enhance image resolution during SEM/EDS analysis, the sample surfaces were coated with a thin layer of gold (Quorum Coater) and grounded via silver paste.

Figure 2. Low-temperature magnetic levitation force measurement system (MLFMS)

The magnetic levitation force measurements of the MgB_2 samples were conducted using a custom-designed low-temperature magnetic levitation force measurement system (MLFMS) (Celik, 2016), developed to operate in the temperature at 20 and 25K (Fig. 2). In this system, a cylindrical NdFeB permanent magnet is positioned beneath the superconducting sample, and its 3D motion (in x, y, and z axes) are precisely controlled by a high-resolution vacuum-compatible XYZ linear stage. The vertical (F_z) and lateral (F_x, F_y) components of the levitation force are recorded in real-time using three orthogonally aligned calibrated beam load cells. The cylindrical NdFeB permanent magnet (grade N52) used in the measurements had a height of 9.8 mm, a diameter of 19.7 mm, and a surface magnetic flux density of 5233 G. The superconducting sample is mounted on a cryostat cold head within a high-vacuum chamber (down to 10^{-7} Torr), and its temperature is monitored and controlled by AlGaAs diodes and a LakeShore 336 temperature controller. Measurements were performed under both field-cooled (FC) and zero-field-cooled (ZFC) regimes. The system allows not only force–distance (F_z–z and F_x–x) and force–temperature (F_z–T) measurements but also enables evaluation of magnetic stiffness by capturing the variation of force with small displacements at fixed temperature.

3. Results and discussion

The X-ray diffraction (XRD) patterns of PAni powder and bulk samples of MgB_2 + x wt% PAni (x = 0, 1.5, 3, 4.5, and 6) in a disk shape with an average diameter of 13 mm and a mass of ~1.5 g are presented in Figure 3. The XRD pattern of powder PAni shows two distinct broad peaks at 24.7° and 43.6°, indicating that polymer chain order exists only over short distances (Ravikiran et al., 2006). It has been determined that both pure and PAni-addition MgB_2 samples grow in a hexagonal crystal structure with a preferred orientation in the (101) plane (JCPDS 00-006-0640). XRD analysis revealed multiple diffraction peaks corresponding to various crystallographic planes of the samples. Specifically, diffraction peaks were observed at ≈2θ = 25.15°, 33.35°, 42.32°, 51.64°, 59.78°, 63.05°, 66.01°, 70.37°, 76.03° and 83.17° which are associated with the (001), (100), (101), (002), (110), (102), (111), (200), (201) and (112) diffraction planes, respectively.

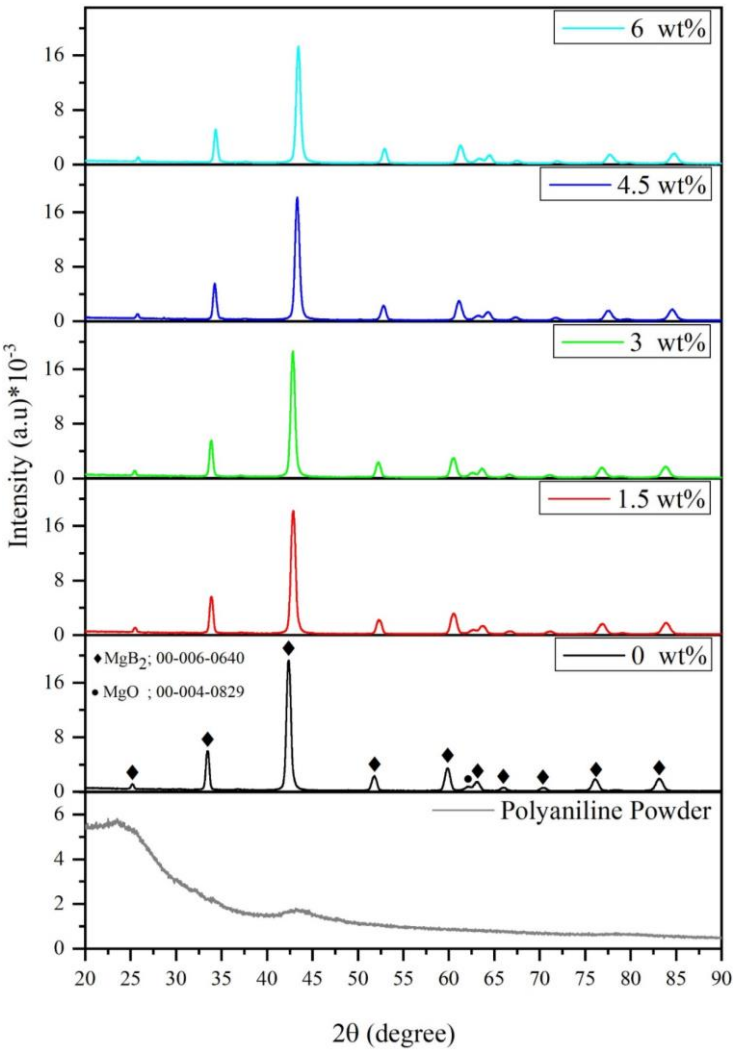

Figure 3. XRD patterns of pure and PAni-addition MgB_2 samples showing the effect of PAni content on phase composition and crystalline.

In addition to the diffraction peaks corresponding to the main MgB_2 phase, minor peaks attributed to the MgO secondary phase were observed at ≈2θ = 62.05° (JCPDS 00-004-0829).

The pure sample (0 wt% PAni) exhibits well-defined peaks characteristic of MgB_2, indicating a high degree of crystallinity. As the PAni content increases, no secondary phase peaks related to polyaniline decomposition or reaction byproducts are observed, suggesting that the addition of PAni up to 6 wt% does not significantly alter the main MgB_2 phase. However, a progressive increase in peak intensity and sharpness, especially for the (100), (101), and (110) reflections, is observed with increasing PAni content, particularly up to 3 wt%. This behavior may indicate improved crystallinity and grain alignment facilitated by the PAni additive during the sintering process (Wang et al., 2012).

At higher addition levels (4.5 wt% and 6 wt%), the XRD peaks remain sharp but exhibit no further substantial enhancement, possibly implying a saturation effect or limited incorporation of PAni-derived components into the MgB_2 matrix.

Overall, the structural results suggest that PAni addition up to a certain threshold may enhance the crystalline quality of MgB_2 without introducing secondary phases, making it a promising route for tailoring microstructural properties.

Figure 4 presents the evolution of the most intense XRD peak of MgB_2, located around 2θ ≈ 42–43°, as a function of increasing PAni content. The diffraction peak corresponding to the (101) plane was closely examined for samples with 0, 1.5, 3, 4.5, and 6 wt% PAni additions to evaluate the influence of PAni on the crystalline quality of the MgB_2 phase.

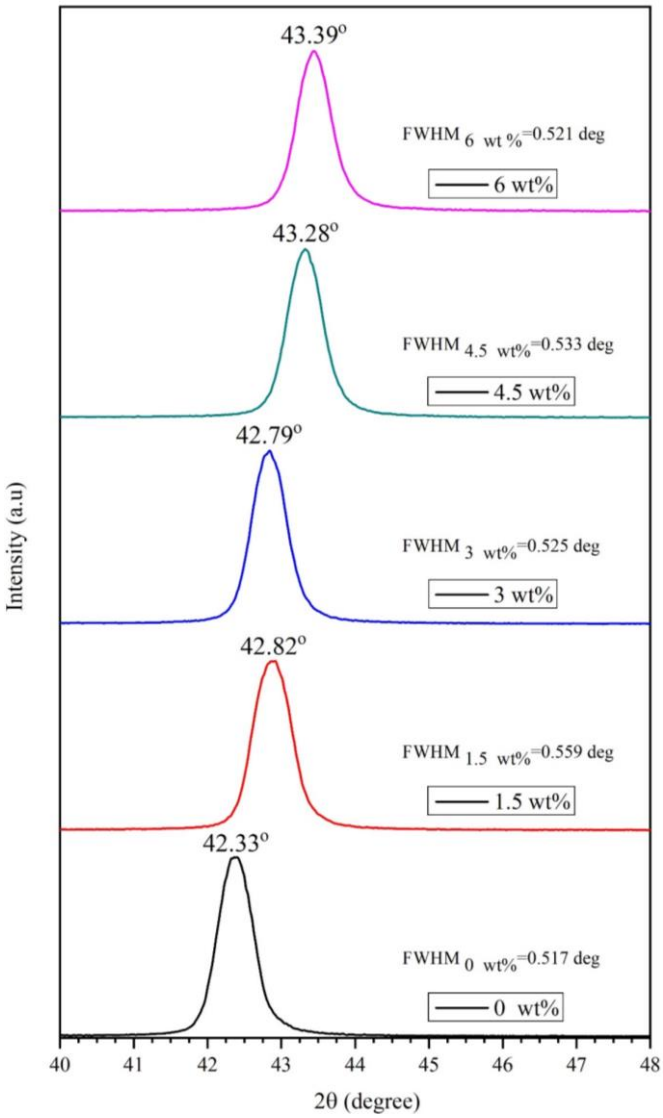

Figure 4. Evolution of the most intense (101) diffraction peak with increasing PAni content, indicating peak shift and broadening used for crystallite size and strain calculations.

A gradual shift in the peak position toward higher 2θ values was observed with increasing PAni content. Specifically, the peak shifted from 42.33° for the pure sample to 43.39° for the 6 wt% PAni-addition sample. In terms of peak broadening, the full width at half maximum (FWHM) values exhibited a non-monotonic trend. The pure MgB_2 sample showed a FWHM of 0.517°, while the values for PAni-addition samples varied between 0.521° and 0.559°. The maximum broadening occurred for the 1.5 wt% PAni sample (FWHM = 0.559°), suggesting increased lattice distortion or reduced crystallite size at this addition level. However, at higher PAni contents (e.g., 6 wt%), the FWHM decreased slightly to 0.521°, indicating a possible recrystallization or grain refinement effect.

The lattice parameters a and c of the hexagonal MgB_2 phase were determined from the X-ray diffraction (XRD) patterns using Bragg's law (equations 1) (Kacher et al., 2009);

$$n\lambda = 2d\sin\theta \tag{1}$$

where n is the order of reflection (taken as 1), λ is the wavelength of the CuKα radiation (1.5406 Å), d is the interplanar spacing, and θ is the Bragg diffraction angle. The d-spacing values for the selected diffraction peaks were calculated directly from the measured 2θ values.

For a hexagonal crystal system, the relation between d_{hkl} (equations 2), a (equations 3-4), and c (equations 5-6) is given by (Aquí-Romero et al., 2020);

$$\frac{1}{d_{hkl}^2} = \frac{4}{3}\frac{h^2+hk+k^2}{a^2} + \frac{l^2}{c^2} \tag{2}$$

a parameter was calculated from the (100) reflection ($l = 0$) as:

$$a = \sqrt{\frac{4}{3}(h^2 + hk + k^2)}d_{hk0} \tag{3}$$

which simplifies for the (100) peak (h=1, k=0) to:

$$a = \sqrt{\frac{4}{3}}d_{100} \tag{4}$$

The c parameter was obtained from the (002) reflection (h=0, k=0) as:

$$c = l \cdot d_{00l} \tag{5}$$

which simplifies for the (002) peak (l=2) to:

$$c = 2 \cdot d_{002} \tag{6}$$

The unit cell volume, V (equations 7) for the hexagonal crystal system was calculated using (He et all., 2005);

$$V = \frac{\sqrt{3}}{2}a^2c \tag{7}$$

The a, b, c, V and d values calculated in accordance with this information are given in Table 1.

Table 1. Lattice parameters (a, b, c), unit cell volume (V), and interplanar spacing d (101) of MgB_2 with different PAni contents

PAni content	a=b (Å)	c (Å)	V (Å^3)	d (101) (Å)
0 wt%	3.0859	3.5304	29.1151	2.1335
1.5 wt%	3.0551	3.4964	28.2620	2.1102
3 wt%	3.0574	3.5009	28.3410	2.1116
4.5 wt%	3.0225	3.4664	27.4247	2.0888
6 wt%	3.0140	3.4596	27.2172	2.0838

Figure 5 shows the variation of lattice parameters (a, c), interplanar spacing d (101), and unit cell volume (V) of MgB_2 as a function of PAni content. Both a and c lattice parameters exhibit a decreasing trend with increasing PAni content. For the pure sample, a parameter is 3.0859 Å, which decreases to 3.0140 Å for the 6 wt% PAni-addition sample. Similarly, the c parameter decreases from 3.5304 Å to 3.4596 Å. This systematic contraction in both lattice parameters leads to a reduction in unit cell volume from 29.1151 $Å^3$ to 27.2172 $Å^3$.

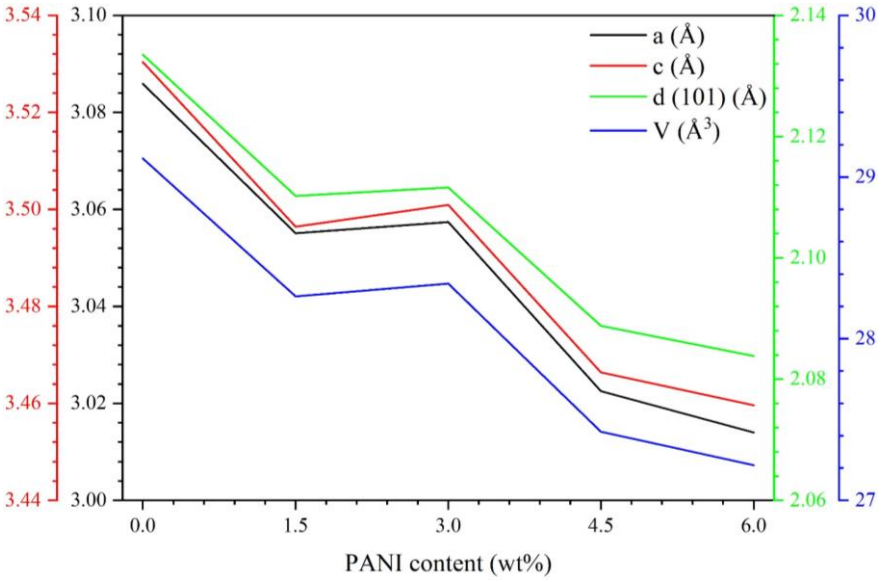

Figure 5. Variation of lattice parameters (a, c), interplanar spacing d (101), and unit cell volume (V) as a function of PAni content, derived from XRD analysis

The interplanar spacing of the (101) plane also decreases with addition, from 2.1335 Å for pure MgB_2 to 2.0838 Å for the 6 wt% PAni-addition sample. This reduction is a clear indication of lattice contraction. Such contraction is typically attributed to carbon substitution at boron sites (C-substitution) in the MgB_2 crystal lattice. During the thermal decomposition of PAni, carbon atoms are released and may replace boron atoms in the MgB_2 lattice. Since the atomic radius of carbon is smaller than that of boron, this substitution causes a decrease in both lattice parameters and the unit cell volume (Cheng et al., 2017).

This structural modification can significantly influence the electronic density of states near the Fermi level, which is crucial for the superconducting properties of MgB_2. Carbon substitution is known to reduce the superconducting transition temperature but may enhance the upper critical field and flux pinning, depending on the addition level (Nanot et al., 2009; Wisniewski et al., 2007). Therefore, the observed structural changes suggest that the superconducting performance of PAni-addition MgB_2 could be tuned through controlled addition.

For a comprehensive assessment of the crystalline quality of the MgB_2 bulk samples, the crystallite size (D) (equations 8), lattice strain (ε) (equations 9), and dislocation density (δ) (equations 10) were calculated based on the following established relations (Aydın Ünal, 2024; Bayazit et al., 2025).

$$D = \frac{0.9\times\lambda}{\beta\times\cos\theta} \tag{8}$$

$$\varepsilon = \frac{\beta\cos\theta}{4} \tag{9}$$

$$\delta = \frac{1}{D^2} \tag{10}$$

where, β denotes the full width at half maximum (FWHM) of each diffraction peak, θ is the Bragg diffraction angle, λ represents the wavelength of the CuKα radiation (0.1504 Å).

Based on the (101) plane corresponding to the orientation of the most intense peak, the crystal size, dislocation density and strain values of the pure and PAni-addition samples are given in Table 2.

Table 2. XRD-derived structural parameters of MgB_2 with different PAni contents, including 2θ, FWHM, D, δ, and ε

Sample	Diffraction Angle, 2θ (°)	FWHM (deg)	Crystallite Size, D (nm)	Dislocation Density, nm^{-2} ($*10^{-3}$)	Strain, ε ($*10^{-3}$)
0 wt%	42.33	0.517	16.47	3.68	5.82
1.5 wt%	42.82	0.559	15.26	4.29	6.22
3 wt%	42.79	0.525	16.25	3.78	5.84
4.5 wt%	43.28	0.533	16.03	3.88	5.86
6 wt%	43.39	0.521	16.41	3.71	5.71

Table 2 presents the crystallite size, dislocation density, and strain values calculated from the XRD peak broadening of pure and PAni-addition MgB_2 samples. The pure sample exhibited the largest crystallite size of 16.47 nm. With the addition of 1.5 wt% PAni, a notable decrease to 15.26 nm was observed, indicating that PAni incorporation may hinder grain growth and promote the formation of smaller crystallites. Similar trends have been reported in the literature, where polymer additives act as grain-growth inhibitors during synthesis processes (Zeng et al., 2008).

Interestingly, further increase in PAni content (3–6 wt%) led to a partial recovery of crystallite size, suggesting that the suppressing effect of PAni on crystallite growth may saturate beyond a certain concentration. This could be attributed to the reorganization of crystal domains or improved crystallization kinetics at higher addition levels (Shahabuddin et al., 2025).

The dislocation density (δ), which is inversely proportional to the square of the crystallite size, was highest in the 1.5 wt % PAni-addition sample (4.29×10^{-3} nm^{-2}), in agreement with its smallest crystallite size (Shahbazi et al., 2023). The increased dislocation density implies a higher density of crystalline defects, which is often associated with enhanced mechanical hardness but can also influence electronic transport properties.

Similarly, microstrain (ε) values increased slightly with adding, peaking again at 1.5 wt% PAni (6.22×10^{-3}). This behavior suggests that PAni addition induces local lattice distortions due to interfacial stress or imperfect incorporation into the MgB_2 lattice, as observed in other added superconducting materials (Deyu et al., 2025). Overall, the results indicate that low levels of PAni adding introduce significant microstructural modifications in MgB_2, particularly by increasing defect density and lattice strain, which may have implications for its superconducting or mechanical properties.

Figure 6 presents the SEM micrographs of MgB2 samples synthesized with different PAni contents (0, 1.5, 3, 4.5, and 6 wt%). The pure (0 wt%) sample exhibits a porous and irregular morphology with large, agglomerated clusters. At 1.5 wt% PAni addition, the surface becomes more uniform with finer grains and reduced porosity. For the 3 wt% and 4.5 wt% samples, partial coalescence of particles and grain boundary smoothing can be observed, indicating improved intergranular connectivity. At 6 wt%, the grains appear more compactly packed, and the pore size is further decreased, suggesting an overall densification of the microstructure.

As shown in the levitation force (F_z) versus distance (z) curves under field-cooled (FC, Fig. 7a-7b) and zero-field-cooled (ZFC, Fig. 7c-7d) conditions, the incorporation of PAni clearly affects the magnetic response of the bulk MgB_2 samples. In the zero-field cooling (ZFC) mode, the superconducting sample is cooled to the desired temperature while placed about 100 mm away from the permanent magnet. Once the temperature is stabilized, the magnet is gradually brought closer to the sample, and the repulsive force arising from the Meissner effect is recorded. The term initial force denotes the maximum repulsive force at the closest distance.

In the field cooling (FC) mode, the sample is cooled below its critical temperature while kept approximately 1.5 mm away from the magnet. Subsequently, the magnet is lifted (up to roughly 50 mm), and the highest measured force corresponds to the peak levitation force under FC conditions.

In FC mode, the repulsive force increased with higher PAni concentration, particularly in the 4.5% and 6% PAni-addition MgB_2 samples, likely indicating enhanced magnetic flux exclusion due to additional flux pinning centers. This observation is consistent with literature reports indicating that MgB_2 addition with magnetic or conductive additives can enhance pinning ability and levitation performance (Tripathi et al., 2021).

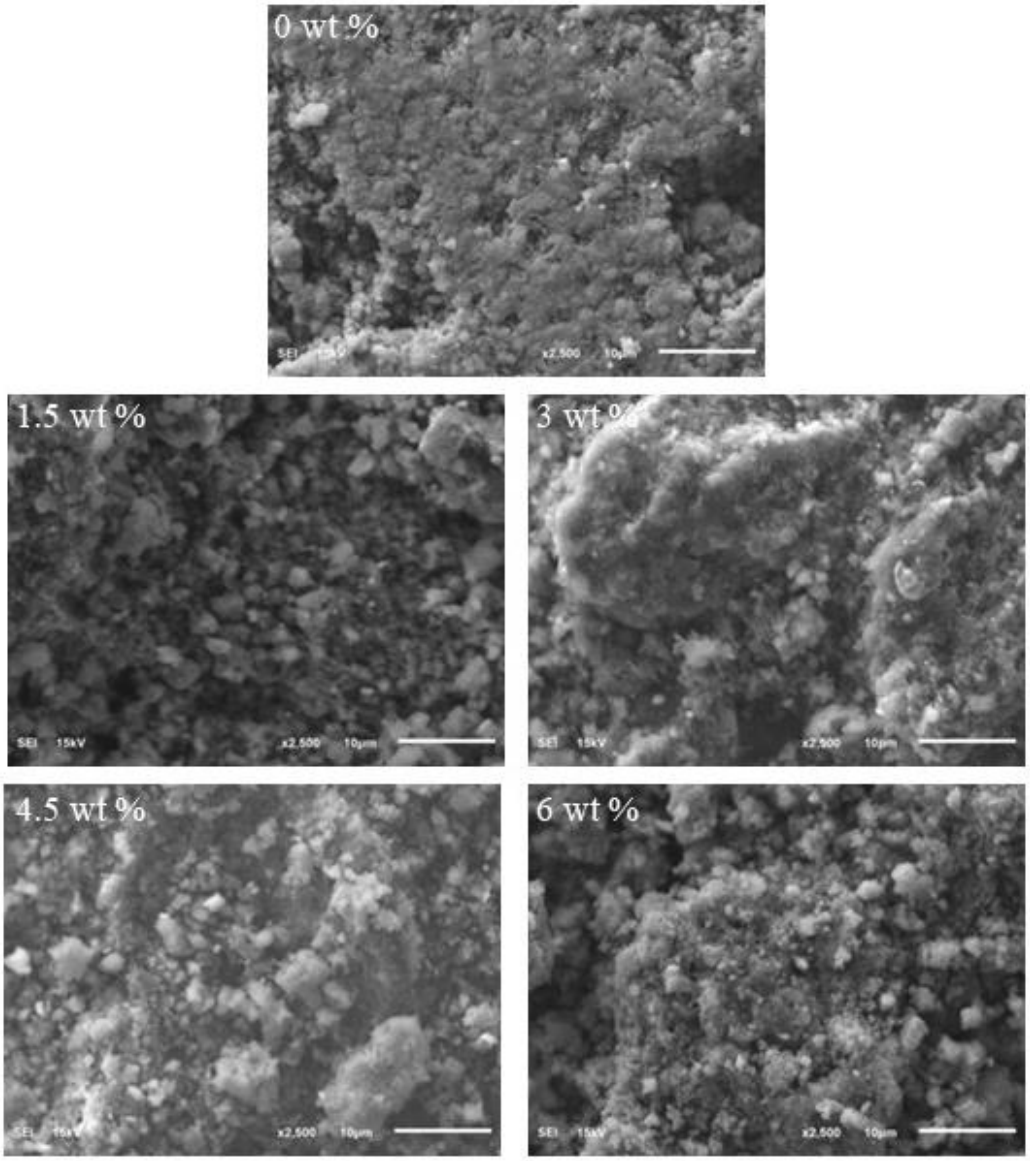

Figure 6. SEM micrographs of MgB_2–PAni samples with different PAni contents showing changes in particle size, porosity, and surface homogeneity

Conversely, under ZFC conditions, samples with higher PAni content exhibited a noticeable decrease in initial levitation force, implying that magnetic flux penetrates the material more easily, likely due to weakened pinning efficiency in the absence of an external field during cooling. This dependence on cooling conditions mirrors findings from MgB_2 studies, where levitation performance varies significantly between the ZFC and FC regimes (Savaşkan et al., 2016; Yanmaz et al., 2010).

In both configurations, stronger levitation forces were recorded at 20 K compared to 25 K, consistent with the expected temperature dependence of flux pinning. Theoretical modeling for high-T_c superconductors shows that as temperature decreases, levitation force initially increases and then tends toward saturation, in line with increased critical current density and pinning strength (Zhou et al., 2010). Similarly, in MgB_2 bulk samples, studies on sintering temperatures demonstrate that enhanced levitation force and electromagnetic performance are achieved at optimized lower temperatures, corroborating the observed increase in pinning efficacy at 20 K versus 25 K (Savaşkan et al., 2021)

These results suggest that while the addition of PAni benefits levitation under FC conditions (this enhancement may be related to improved grain connectivity and microstructural refinement), it may be detrimental to initial force performance under ZFC. For comparison, other additives, such as carbon or nano-boron, were found to selectively enhance repulsive or attractive forces depending on the additive type and measurement configuration (Duz et al., 2018).

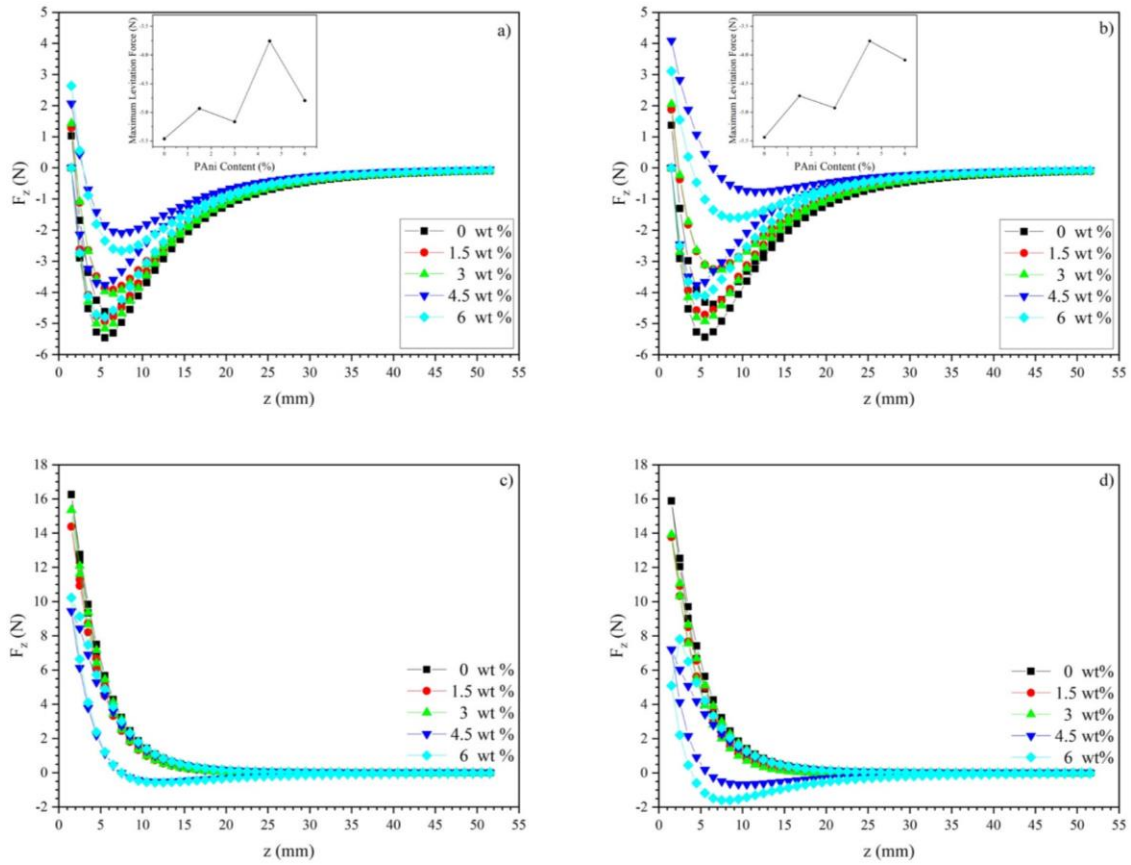

Figure 7. F_z versus - z-direction distance for MgB_2–PAni samples at 20 K (a), 25 K (b) under FC regime and at 20 K (c), 25 K (d) under ZFC regime, Inset illustrates (a and b) maximum levitation force values versus different PAni contents.

The inset graphs in Figure 7a and b illustrate the variation of the maximum levitation force with PAni content. The levitation force initially increases up to 3 wt% PAni, indicating enhanced flux pinning and improved intergranular coupling due to the presence of finely dispersed polymer phases. Beyond this concentration, a slight decrease is observed, which may be attributed to the excessive PAni phase accumulating at grain boundaries and partially suppressing superconducting connectivity. This non-linear behavior suggests that an optimal PAni concentration exists around 3 wt%, where the balance between improved pinning and structural uniformity results in maximum magnetic performance.

4. Discussion and conclusions

The experimental results reveal a clear correlation between the lattice parameter contraction induced by PAni addition and the variation in levitation force. As PAni content increases, both a and c parameters systematically decrease, accompanied by a reduction in unit cell volume. This contraction is attributed to partial carbon substitution from PAni decomposition, which replaces boron atoms in the MgB_2 lattice. Such substitution modifies the electronic density of states and flux pinning behavior. The FC levitation measurements indicate that moderate contraction (observed at ~4.5–6 wt% PAni) coincides with a noticeable enhancement in maximum levitation force, likely due to improved grain connectivity and additional pinning centers. Conversely, ZFC results show a reduction in initial levitation force at higher addition levels, suggesting facilitated flux entry under zero-field cooling. Overall, the data indicates that structural modifications at the atomic scale directly influence magnetic levitation performance in PAni-addition MgB_2 samples.

Acknowledgement

The author would like to express sincere gratitude to Professor Burcu Savaşkan and Dr. Vildan Erduran for their support in material procurement, to Associate Professor Sait Barış Güner for his contributions to the production process and levitation measurements, and to Professor Şükrü Özçelik for manufacturing the levitation system.

Declaration of ethical code

The authors of this article declare that the materials and methods used in this study do not require ethics committee approval and/or legal-special permission.

Conflicts of interest

The authors declare that they have no conflicts of interest in the publication.

References

Aquí-Romero, F., Willars-Rodríguez, F. J., Chávez-Urbiola, I. R., & Ramírez-Bon, R. (2020). ZnO_2 films by successive ionic layer adsorption and reaction method and their conversion to ZnO ones for p-Si/n-ZnO photodiode applications. *Semiconductor Science and Technology*, *35*(2). https://doi.org/10.1088/1361-6641/ab5f2a

Aydın Ünal, F. (2024). Nadir toprak elementi (Gd) katkılı ZnO nanoparçacıkların sol-jel yöntemi ile sentezlenmesi ve karakteristik özelliklerinin incelenmesi. *Afyon Kocatepe University Journal of Sciences and Engineering*, *24*(2), 424–433. https://doi.org/10.35414/akufemubid.1371091

Bayazit, T., Kanmaz, İ., Tomakin, M., & Üzüm, A. (2025). Triple layer $TiO_2/HfO_2/SiO_2$ thin film design for reduction of optical losses. *Physica Scripta*, *100*(4). https://doi.org/10.1088/1402-4896/adc049

Braccini, V., Nardelli, D., Penco, R., & Grasso, G. (2007). Development of ex situ processed MgB_2 wires and their applications to magnets. In *Physica C: Superconductivity and its Applications* (Vol. 456, Issues 1–2, pp. 209–217). https://doi.org/10.1016/j.physc.2007.01.030

Celik, S. (2016). Design of magnetic levitation force measurement system at any low temperatures from 20K to room temperature. *Journal of Alloys and Compounds*, *662*, 546–556. https://doi.org/10.1016/j.jallcom.2015.11.230

Cheng, C., Reddy, K. M., Hirata, A., Fujita, T., & Chen, M. (2017). Structure and mechanical properties of boron-rich boron carbides. *Journal of the European Ceramic Society*, *37*(15), 4514–4523. https://doi.org/10.1016/j.jeurceramsoc.2017.06.017

Deyu, G. K., Wenskat, M., Díaz-Palacio, I. G., Blick, R. H., Zierold, R., & Hillert, W. (2025). Recent advances in atomic layer deposition of superconducting thin films: a review. *In Materials Horizons. Royal Society of Chemistry*, *12*, 5594-5626. https://doi.org/10.1039/d5mh00323g

Duz, I., Guner, S. B., Erdem, O., Demir, I., Kapucu, V., Çelik, Ş., Ozturk, K. Hossain, S., Gencer, A., & Yanmaz, E. (2014). Comparison of levitation forces of bulk MgB_2 superconductors produced by nano boron and carbon-doped nano boron. *Journal of Superconductivity and Novel Magnetism*, *27*(10), 2241-2247. https://doi.org/10.1007/s10948-014-2602-4

Erdem, O., Guner, S. B., Celik, S., & Kucukomeroglu, T. (2020). Superconducting and levitation force characterisation of pyrene added MgB_2 bulk superconductors. *Cryogenics*, *112*. https://doi.org/10.1016/j.cryogenics.2020.103205

Güner, S. B. (2020). Effects of silver doping on magnetic levitation performance of MgB_2 superconductors. *Cryogenics*, *108*. https://doi.org/10.1016/j.cryogenics.2020.103061

He, X., & Jia, W. (2005). Hexagonal structure for intelligent vision. In 2005 International conference on information and communication technologies (ICICT) (pp. 52-64), Pakistan. doi: 10.1109/ICICT.2005.1598543

Kacher, J., Landon, C., Adams, B. L., & Fullwood, D. (2009). Bragg's Law diffraction simulations for electron backscatter diffraction analysis. *Ultramicroscopy*, *109*(9), 1148–1156. https://doi.org/10.1016/j.ultramic.2009.04.007

Nagamatsu, J., Nakagawa, N., Muranaka, T., Zenitani, Y. & Akimitsu, J., (2001). Superconductivity at 39 K in magnesium diboride. *Nature*, 410(6824), 63-64. https://doi.org/10.1038/35065039

Nanot, S., Avriller, R., Escoffier, W., Broto, J. M., Roche, S., & Raquet, B. (2009). Propagative Landau states and Fermi level pinning in carbon nanotubes. *Physical Review Letters*, *103*(25). https://doi.org/10.1103/PhysRevLett.103.256801

Prasanna, B. P., Avadhani, D. N., Muralidhara, H. B., Chaitra, K., Thomas, V. R., Revanasiddappa, M., & Kathyayini, N. (2016). Synthesis of polyaniline/ZrO_2 nanocomposites and their performance in AC conductivity and electrochemical supercapacitance. *Bulletin of Materials Science*, *39*(3), 667–675. https://doi.org/10.1007/s12034-016-1196-9

Ravikiran, Y. T., Lagare, M. T., Sairam, M., Mallikarjuna, N. N., Sreedhar, B., Manohar, S., MacDiarmid, A. G., & Aminabhavi, T. M. (2006). Synthesis, characterization and low frequency AC conduction of polyaniline/niobium pentoxide composites. *Synthetic Metals*, *156*(16–17), 1139–1147. https://doi.org/10.1016/j.synthmet.2006.08.005

Savaskan, B. (2021). The Investigation of In-Situ Processed MgB_2 on Bulk Electromagnetic Behaviour by Numerical and Experimental Methods. *Available at SSRN 3980029*.

Savaşkan, B., Koparan, E. T., Güner, S. B., Öztürk, K., & Çelik, Ş. (2019). Enhanced magnetic levitation and guidance force in MgB_2 bulks by synthetic engine oil immersion. *Journal of Superconductivity and Novel Magnetism*, *32*(4), 827–837. https://doi.org/10.1007/s10948-018-4775-8

Savaskan, B., Koparan, E. T., Güner, S. B., Celik, S., & Yanmaz, E. (2016). The size effect on the magnetic levitation force of MgB_2 bulk superconductors. *Cryogenics*, *80*, 108-114. https://doi.org/10.1016/j.cryogenics.2016.09.013

Shadab, M., & Miryala, M. (2024). Tuning grain boundaries in MgB_2 through boron ultra-sonication in 1-heptanol. *Ceramics International*, *50*(13), 22266–22277. https://doi.org/10.1016/j.ceramint.2024.03.259

Shahabuddin, M., Alzayed, N. S., Madhar, N. A., Qaid, S. A., & Ramay, S. M. (2025). Impact of Carbon-Based Doping on the Structural and Superconducting Properties of MgB2: A Comparative Study. *Journal of Superconductivity and Novel Magnetism*, 38(2), 102. https://doi.org/10.1007/s10948-025-06942-7

Shahbazi, M., Pannu, A. S., Alarco, J., Sonar, P., & Mackinnon, I. (2023). Impact of hair-derived carbon substitution on structural and superconducting properties of MgB_2. *AIP Advances*, *13*(12). https://doi.org/10.1063/5.0174642

Shumaila, Alam, M., Siddiqui, A. M., & Husain, M. (2014). A study on the synthesis, characterization and properties of polyaniline/magnesium boride nanocomposites. *Polymer International*, *63*(8), 1465–1470. https://doi.org/10.1002/pi.4643

Shumaila, D., Zulfequar, M., & Husain, M. (2017). Synthesis, characterization and properties of MgB_2 doped polyaniline. *Journal of Modern Materials*, *4*(1), 1–9. https://doi.org/10.21467/jmm.4.1.1-9

Shumaila, Habib, H., Singh, G., Husain, M., Zulfequar, M., & Husain, S. (2019). Facile field emission characteristics of polyaniline doped with MgB_2 nanowires. *Materials Research Express*, *6*(10). https://doi.org/10.1088/2053-1591/ab3759

Soysal, F., & Çıplak, Z. (2023). Grafen oksit/altın/polianilin nanokompozitlerinin eş zamanlı çöktürme/polimerizasyon yöntemleriyle sentezi ve fototermal performansı. *Afyon Kocatepe University Journal of Sciences and Engineering*, *23*(5), 1246–1255. https://doi.org/10.35414/akufemubid.1252385

Stejskal, J. & Gilbert, R. G. (2002). Polyaniline, preparation of a conducting polymer. Pure and applied chemistry, 74(5), 857-867. https://doi.org/10.1351/pac200274050857

Tripathi, D., Bhatnagar, A., Raj, S., Rai, D. K. & Dey, T. K. (2021). Levitation force of graphene added bulk MgB_2 superconductor. *Cryogenics*, *118,* 103343, 0011-2275. https://doi.org/10.1016/j.cryogenics.2021.103343

Wang, Y., Li, X., & Li, C. (2012). One-dimensional nanostructured polyaniline: syntheses, morphology controlling, formation mechanism, and applications. *Advances in Polymer Technology*, 31(4), 319–330. https://doi.org/10.1002/adv.2128

Wisniewski, A., Puzniak, R., Judek, J., Krutzler, C., Eisterer, M., Weber, H. W., Jun, J., Kazakov, S. M., & Karpinski, J. (2007). Comparison of the influence of carbon substitution and neutron-induced defects on the upper critical field and flux pinning in MgB_2 single crystals. *Superconductor Science and Technology*, *20*(3), 256–260. https://doi.org/10.1088/0953-2048/20/3/025

Xi, X. X. (2008). Two-band superconductor magnesium diboride. *Reports on Progress in Physics*, *71*(11). https://doi.org/10.1088/0034-4885/71/11/116501

Yanmaz, E., Ozturk, K., Dancer, C. E., Basoglu, M., Celik, S., & Grovenor, C. R. M. (2010). Levitation force at different temperatures and superconducting properties of nano-structured MgB_2 superconductors. *Journal of alloys and compounds*, *492*(1-2), 48-51. https://doi.org/10.1016/j.jallcom.2009.11.177

Zeng, R., Lu, L., & Dou, S. X. (2008). Significant enhancement of the superconducting properties ofMgB2 by polyvinyl alcohol additives. *Superconductor Science and Technology*, *21*(8), 085003. https://doi.org/10.1088/0953-2048/21/8/085003

Zhang, H., Zhao, Y., & Zhang, Y. (2015). The Effects of Excess Mg Addition on the Superconductivity of MgB_2. *Journal of Superconductivity and Novel Magnetism*, *28*(9), 2711–2714. https://doi.org/10.1007/s10948-015-3120-8

Zhou, J., Zhang, X. Y., & Zhou, Y. H. (2010). Temperature dependence of levitation force and its relaxation in a HTS levitation system. *Physica C: Superconductivity*, *470*(5-6), 336-339. https://doi.org/10.1016/j.physc.2009.12.070